

## Photophysics and Photochemistry of Thymine Deoxy-Dinucleotide in Water: A PCM/TD-DFT Quantum Mechanical Study

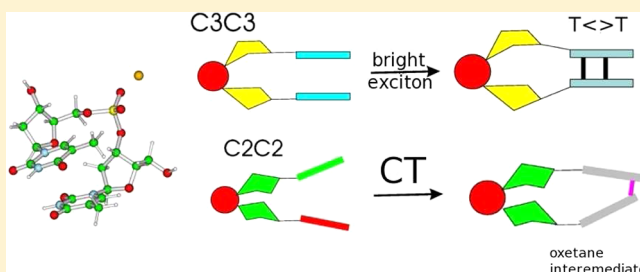
Roberto Improta\*

CNR-Consiglio Nazionale delle Ricerche, Istituto di Biostrutture Biomagini (IBB-CNR), Via Mezzocannone 16, I-80134 Napoli, Italy

## Supporting Information

**ABSTRACT:** We here report a fully quantum mechanical study of the main photochemical and photophysical decay routes in aqueous solution of thymine deoxy-dinucleotide (TpT<sup>−</sup> and TpTNa) and of its analogue locked in C3-endo puckering, characterizing five different representative backbone conformers and discussing the chemical physical effects modulating the yield of the different photoproducts. Our approach is based on time-dependent DFT calculations, using the last generation M052X functional, whereas solvent effects are included by means of the polarizable continuum model.

Especially when at least one of the sugars adopts C3-endo puckering, a barrierless path on the bright  $\pi\pi^*$  excitons leads to the  $S_1/S_0$  crossing region corresponding to the formation of cyclobutane pyrimidine dimer. Charge transfer excited states involving the transfer of an electron from the 5' Thy toward the 3' Thy are involved in the formation of the oxetane intermediate in the path leading to 6-4 pyrimidine pyrimidinone adducts. A non-negligible energy barrier is associated with this latter pathway, which is possible only when one of the two nucleotides adopts C2-endo puckering. Monomer-like decay pathways, involving  $\pi\pi^*$  or  $n\pi^*$  excited states localized on a single base, are shown to be operative also for loosely stacked bases.



## 1. INTRODUCTION

Irradiation of DNA with ultraviolet (UV) light triggers a cascade of photochemical events, which are potentially dangerous because they can lead to the damage of the genetic code and, ultimately, to apoptosis and carcinogenesis.<sup>1,2</sup> The most frequent phototolesions involve two stacked pyrimidine bases, especially thymine (T), providing the formation of cyclobutane pyrimidine dimers (T<>T) and 6-4 pyrimidine pyrimidinone adducts (6-4TT) (Figure 1), the formation yield of T<>T being  $\sim 1$  order of magnitude larger than that of 6-4TT.<sup>1</sup> Due to its biological relevance the dimerization process has been extensively studied, by both experimental and computational approaches.<sup>3–21</sup> Ultrafast time-resolved spectroscopic experiments on (dT)<sub>18</sub> single strands and on thymidine deoxydinucleotide (TpT) indicate that the T<>T lesion is formed in  $\sim 1$  ps,<sup>3,4</sup> suggesting that T<>T is formed via a singlet pathway and that its formation is ruled by the oligonucleotide ground state conformation; i.e., the few percent of base pairs with the suitable stacking geometry react almost quantitatively. On the other hand, it has been proposed that a major precursor for T<>T photodamage is a triplet state, accessed via an intermediate state, resulting from the vibronic interaction between the bright  $\pi\pi^*$  and the dark  $n\pi^*$  states of T.<sup>11</sup> The involvement of triplet would be supported by the well-documented T<>T formation in the presence of photosensitizers.<sup>1,12</sup>

The photodimerization yield seems to depend also on the sugar conformation. Locked analogues (Figure 1), where a

methylene clamp forces the sugar to adopt a C3-endo conformation, exhibit a much larger T<>T photodimerization yield than oligonucleotide, without forming 6-4TT dimers.<sup>13,19</sup> O-Methyl ether dinucleotide analogues, adopting preferentially, but not exclusively, a C3-endo conformation with a larger fraction of stacked molecules, exhibit instead a 3-fold increase of both T<>T and 6-4TT yield with respect to TpT.<sup>14,15</sup> These latter results have been interpreted as a confirmation of the “singlet, conformationally ruled” mechanism, which is supported also by several studies exploiting molecular dynamics simulations.<sup>17,20</sup>

These interesting studies highlighted the importance of the ground state conformation on the photoisomerization yield, suggesting that the T<>T reaction is modulated by the distance between the midpoints of the reacting C5C6 bonds ( $d$ ) whereas the 6-4TT yield by the C4–O8' distance ( $g$ ) (Figure 1). In different systems single distance cutoff values for  $d$  (3.52 Å) and for  $g$  (2.87 Å), chosen on the ground of the structures issuing from MD simulations, provide indeed good agreement between the predicted and the computed T<>T and 6-4TT yields.<sup>17–20</sup> On the other hand, the role played by other factors (as the dihedral formed by the two reacting CC bonds,  $\eta$ ) is still controversial.<sup>17,20</sup> Furthermore, discrepancies are found between the computed and the predicted 6-4TT yield for some

Received: September 20, 2012

Revised: November 6, 2012

Published: November 7, 2012

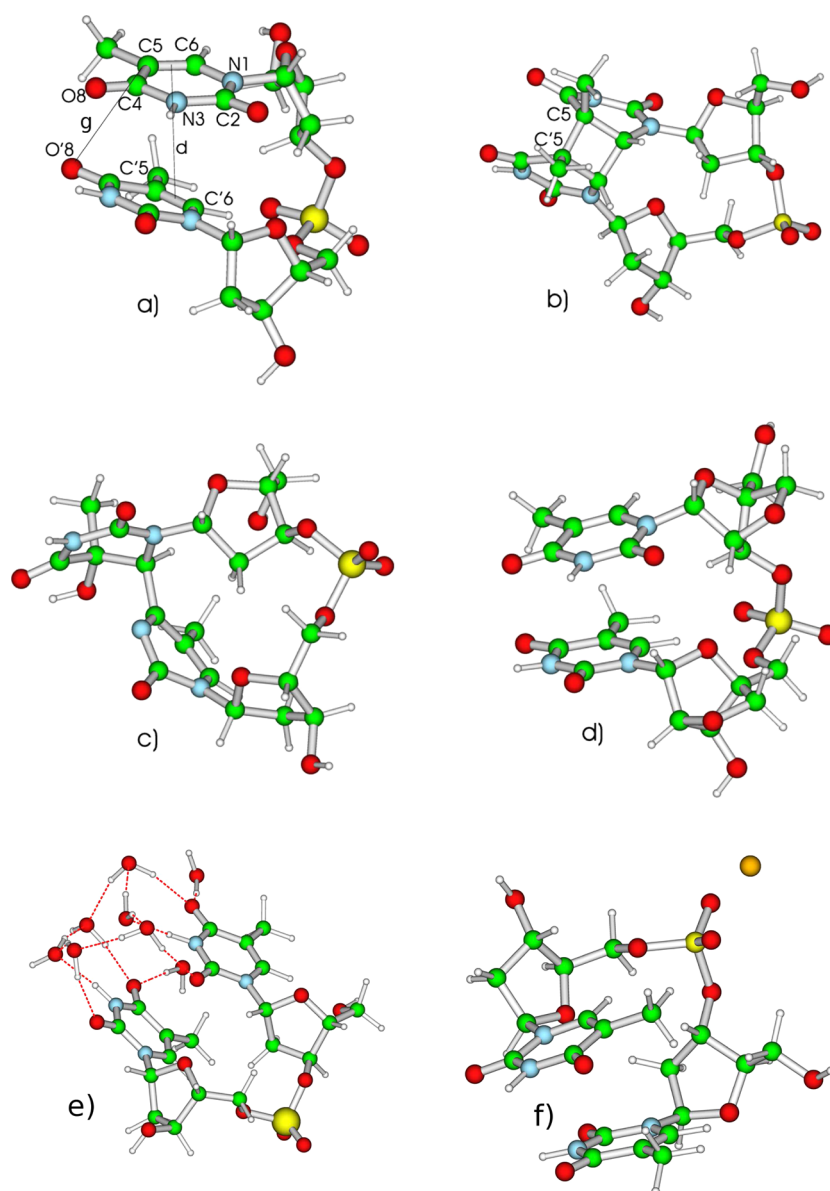


**Figure 1.** Schematic drawing and atom labeling of the systems investigated in the present study: (a) thymine deoxy-dinucleotide (TpT); (b) cyclobutane dimer ( $T \leftrightarrow T$ ); (c) 6-4TT; (d) locked analogue of TpT ( $TpT_L$ ); (e) thymine deoxy-dinucleotide including 8 water molecules ( $TpT \cdot 8(H_2O)$ ); (f) TpT deoxy-dinucleotide including  $Na^+$  counterion ( $TpTNa$ ).

compounds, suggesting that other factors besides those for  $g$  could modulate the formation of 6-4TT.<sup>19,20</sup> There is general consensus that the reaction leading to 6-4TT proceeds through an oxetane stable intermediate (oxet), formed by a Paterno–Büchi reaction,<sup>30</sup> which has been suggested to be formed via  $n\pi^*$  excited states.<sup>16</sup> A recent study<sup>31</sup> also suggests that  $T \leftrightarrow T$  and 6-4TT originate from different excited states:  $T \leftrightarrow T$  from the lowest energy exciton state, 6-4TT from a state with  $T \rightarrow T$  charge transfer (CT) character ( $TT_{CT}$ ).

The number of quantum mechanical (QM) calculations tackling the study of T dimer photophysics is quite limited.<sup>23–28</sup> Multiconfigurational QM studies on the T stacked dimer in the gas phase find that on the lowest energy exciton state (delocalized over the two bases) a barrierless path connects the Franck–Condon (FC) region to a conical intersection (CI) with  $S_0$  ( $CI_{T \leftrightarrow T}$ ), whose structure is similar to that found for ethylene photocycloaddition.<sup>23–25</sup> From  $CI_{T \leftrightarrow T}$  the system can effectively decay to  $T \leftrightarrow T$  (or revert to

the reactants). Another CASPT2/CASSCF study indicates that an excited state with  $T \rightarrow T$  charge transfer character decays to a CI similar to oxet.<sup>24</sup> On the other hand, the energy of  $T \rightarrow T$  in the FC region is rather high (it corresponds to  $S_7$ ).<sup>24</sup>

Other DFT and TD-DFT studies<sup>28,29</sup> indicate a small energy barrier for the  $T \leftrightarrow T$  formation on the singlet state and suggest the possible involvement of triplet state for the formation of 6-4TT.

It is thus clear that, although several of the factors modulating the photochemical reactivity of polythymine single strand have been discovered, a number of important questions are still open: all the low-lying excited states of oligo-Thy, singlet  $\pi\pi^*$ ,  $n\pi^*$ , CT states and triplets have been proposed to be involved in the photochemistry. In particular, from the theoretical point of view, to the best of our knowledge, the role of the backbone and of the solvent has never been analyzed in detail, although the sugar conformation plays a fundamental role in TpT photochemistry and environmental effects can

deeply affect the relative energy of the different excited states.<sup>31</sup> Furthermore, the excited states of the locked TpT analogues have never been investigated, despite their importance for the understanding of the photodimerization mechanism.<sup>13,19</sup> Finally, it is important to study “on the same foot” photochemical and photophysical (i.e., leading to excited state nonreactive deactivation) paths because they are obviously competitive.<sup>32–37</sup> The photophysics of isolated T and thymidine-monophosphate (TMP) have been thoroughly investigated, by both experiments<sup>37</sup> and calculations.<sup>38</sup> Although there is still disagreement on the possible involvement of dark  $n\pi^*$  excited states in the photoactivated dynamics,<sup>38,39</sup> the ultrafast ground state recovery is usually ascribed to a barrierless path on the lowest energy  $\pi\pi^*$  state connecting the Franck–Condon region with an effective CI with the ground electronic state ( $S_0$ ). Stacking interactions could, however, modify the static and dynamical behavior of T bright excited states and it is therefore important to study the interplay between reactive and nonreactive excited state pathways.

To tackle the above issues, we performed a thorough study of the excited state reactivity of TpT and of its analogue where the sugar rings are locked in 3' endo conformation by a methylene bridge (TpT<sub>i</sub>) (Figure 1). Specifically, we have examined five different conformers for TpT: C3(endo),C3'(endo) conformer (hereafter TpT-c3c3) where both sugar rings adopts the C3 endo puckering, C2(endo),C2'(endo) conformer (TpT-c2c2), C2(endo),C3'(endo) (TpT-c2c3), and C3(endo),C2'(endo) (TpT-c3c2), and finally, another conformer where the 5' nucleotide adopts a C2 endo conformation and the 3' one a conformation where both C2 and C3 carbon atoms lies in the sugar average plane, whereas the C1 atom is out of the plane (C2(endo)-C1'(exo), hereafter TpT-c2c1). For TpT<sub>i</sub> only the C3(endo),C3'(endo) has been considered. We investigate the monoanionic form of TpT and consider, for most of the systems, also the effect of the counterion, studying species containing a Na<sup>+</sup> ion (TpTNa) (see Figure 1).

For every conformer examined we have computed the absorption and the electronic circular dichroism (ECD) spectra, to characterize the electronic states in the FC region. The main excited state paths have then been explored, optimizing the geometry of the eight lowest energy excited states. Our calculations are rooted in the time-dependent density functional theory (TD-DFT) and will be based on the M052X functional, whereas the solvent effect will be included by the polarizable continuum model (PCM). This approach has been already successfully applied to the study of oligonucleotides<sup>40–44</sup> and provides a description of the photochemical paths of T dimer in the gas phase in very good agreement with the available multiconfigurational ab initio methods.<sup>31</sup>

Our study provides a global picture of the main photochemical and photophysical decay pathways involving a T stacked pair, indicating that T<>T and 6-4TT photoproducts originate from different excited states and are modulated by different chemical physical effects. Different conformers exhibit a different photochemical reactivity (rationalizing the experimental photoproduct yield) and backbone conformation modulates the excited state behavior in a more subtle way than only affecting the distance between the photoactive moieties.

## 2. COMPUTATIONAL DETAILS

**2.1. Density Functional.** Most of our analysis has been performed by using the M052X functional,<sup>45</sup> which allows an accurate treatment of dispersion interactions<sup>46,47</sup> (and therefore a reliable description of stacked systems) and, at difference with “standard” density functionals,<sup>48</sup> does not significantly overestimate the stability of CT transitions. For example, when interstrand or intrastrand CT transitions are studied,<sup>40–44</sup> M052X provides results in good agreement with CC2 and CASPT2 methods.<sup>49,50</sup> Concerning intrastrand adenine → adenine CT transitions, the M052X prediction<sup>41</sup> is within 0.2 eV of those obtained at the CC2 level,<sup>49</sup> and for adenine → thymine interstrand CT states<sup>42</sup> within 0.25 eV of the CC2 prediction.<sup>50</sup>

More in general, it provides a reliable description of the lowest energy excited states of T in solution<sup>41,51</sup> and a good estimate of the effect of stacking and hydrogen bonding interactions on the excited state properties,<sup>40–44</sup> as shown by the very good agreement with the experimental absorption and ECD spectra (see below). In some cases the M052X analysis has been complemented with the results obtained using other functionals, namely PBE0<sup>52</sup> and M062X.<sup>53</sup> Ground state geometry optimizations, in which all the intramolecular and intermolecular degrees of freedom were fully unconstrained, have been performed at the PCM/M052X/6-31G(d) level. The effect of basis set extension on the absorption and emission energies has been estimated by test geometry optimization and single point computations with more extended 6-31+G(d,p) basis set.

**2.2. Solvent Effect.** Bulk solvent effects have been included by the polarizable continuum model (PCM),<sup>54,55</sup> whereas the effect of solute–solvent hydrogen bonds has been checked by test calculations on a model including eight water molecules of the first solvation shell. Excited state geometry optimizations in solution have been performed by using the “standard” LR (linear-response) implementation of PCM/TD-DFT, for which analytical gradients are available.<sup>56</sup> We also resorted to the state-specific (SS) implementation of PCM/TD-DFT,<sup>57,58</sup> which, when compared to LR-PCM/TD-DFT, provides a more balanced description of solvent effects on different excited electronic states and a significantly more accurate evaluation of the stability of CT transitions.

To get an estimate of the effect of dynamical solvent effects on the paths (especially on that leading to 6-4TT formation), we have characterized the most relevant point of the Potential Energy Surface (PES) by performing both nonequilibrium (neq) and equilibrium (eq) SS-PCM calculations. The equilibrium regime is reached when both fast and slow degrees of freedom are equilibrated with the excited state electron density, whereas in the neq regime only solvent electronic polarization is in equilibrium with the excited state electronic density of the solute (see Supporting Information for details). LR-PCM geometry optimizations have been performed in the neq limit, which is more suitable to treat subpicosecond dynamics (as that involved in the T<>T formation) and it is less prone to overestimation of oscillator strengths than eq calculations.<sup>57</sup> We have, however, checked by performing test eq optimizations that the main conclusions of our study do not depend on the solvent time-regime used in geometry optimizations.

The dimension of the systems and its flexibility make difficult a proper treatment of vibrational effects on the absorption



spectra, and we have followed to the procedure outlined below. The computed stick spectra of  $\text{TMP}^{2-}$  has been convoluted by a Gaussian with half-width half-maximum (HWHM) of 0.2 eV, to model purely vibrational effects on the spectra. The 0.2 value has been chosen to match the width of the experimental spectra of TMP,  $\sim 10\,000\text{--}11\,000\text{ cm}^{-1}$ .<sup>59</sup> To estimate the inhomogeneous broadening associated with each electronic transition, we resorted to a recently developed procedure,<sup>60</sup> in which the inhomogeneous broadening is computed from the solvent reorganization energy  $\lambda$ , according to the proposal of Marcus.<sup>61</sup>  $\lambda$  can be computed from SS-PCM/TD-DFT calculations in the equilibrium and nonequilibrium regimes.<sup>60</sup> The  $\lambda$  value associated with “neutral” exciton is almost vanishing ( $\sim 100\text{ cm}^{-1}$ ) resulting in a very low inhomogeneous broadening ( $<0.1\text{ eV}$ ), i.e., with a negligible contribution to the spectral width. The  $\lambda$  value associated with transition with CT character is instead rather large: for TpT-c2c2 it is  $\sim 0.70\text{ eV}$ , providing an extra contribution to the width of the Gaussian used to convolute the spectra (0.35 eV HWHM, total HWHM 0.4 eV).

**2.3. Crossing Regions.** Although several studies show that for some systems TD-DFT can provide fairly reliable estimate of the geometry and the energy of minimum energy CI,<sup>63</sup> TD-DFT calculations cannot be expected to provide an accurate description of a system in the proximity of a CI with  $S_0$ .<sup>64,65</sup> As a consequence, we have validated our approach by performing a thorough comparison with the results provided for T dimer in the gas phase by accurate MC-SCF calculations.<sup>31</sup> Our analysis indicates that the picture of the photodimerization process provided by TD-M052X on the T dimer in the gas phase is very similar to that obtained at the CASPT2<sup>24,25</sup> level for what concerns the formation of both  $T < > T$  and oxet, not only at the qualitative but also on a quantitative level.<sup>31</sup> The absorption energy of two thimines at the B-DNA is 0.3 eV higher at the TD/M052X/6-31+G(d,p) than at the CASPT2 level,<sup>25</sup> but then the  $S_1$  PES are almost parallel. Both methods predict the passage through a low-energy gradient region 1 eV more stable the FC point (0.96 eV at the CASPT2 level) and then to a CI with  $S_0$  (more stable than the FC point by 1.33 and 1.22 eV at the TD-M052X and at the CASPT2 level, respectively) leading to  $T < > T$  formation.

TD-M052X calculations can be therefore considered fully adequate to the purposes of the present study, which is not to provide a detailed quantum dynamical treatment of the photodimerization process (a task that would be, in any case, out of reach for a dinucleotide in solution, although extremely promising approaches have been recently used<sup>66</sup>) but only qualitative insights on the possible reactive paths in a dinucleotide.

The excited states have been characterized by computing their electric dipole moment, the formal charge present on each atom and on each  $m$  monomer ( $Q_m$ ), and the quantities  $v_m^n$ , related to the variation of the Mulliken atomic populations associated with the electronic transition (see Supporting Information).

All the calculations have been performed by the Gaussian09 Program.<sup>62</sup>

A more detailed description of our computational approach and a discussion of its expected accuracy can be found in the Supporting Information.

### 3. RESULTS

#### 3.1. Absorption Spectrum of TpT and Its Analogues.

##### 3.1.1. TMP Monomer. PCM/M052X/6-31G(d) calculations on

$\text{TMP-H}^-$  and  $\text{TMP}^{2-}$  provide a very similar picture: in agreement with previous computational studies,<sup>32–34,38</sup> two excited states, a dark one with a  $n\pi^*$  (HOMO–1  $\rightarrow$  LUMO) character (hereafter  $T_n$ ) and a bright one with  $\pi\pi^*$  (HOMO  $\rightarrow$  LUMO) character ( $T_\pi$ ), lie close in energy in the FC region (Table 1).  $T_n$  is predicted to be more stable than  $T_\pi$  by  $\sim 0.1$

**Table 1. Absorption Energies ( $\nu_A$ , eV) and Oscillator Strength (au) of the Two Lowest Energy Excited States of  $\text{TMP}^{2-}$  and  $\text{TMP-H}^-$  in Aqueous Solution According to PCM/TD-M052X/6-31G(d) Calculations on PCM/M052X/6-31G(d) Optimized Geometries (Using Gaussian03 Defaults)**

	TMP		TMP-H	
	$T_n$	$T_\pi$	$T_n$	$T_\pi$
LR-PCM Results				
VEE	5.22	5.34	5.20	5.39
osc st	0.00	0.31	0.00	0.32
SS-PCM Results				
VEE SS (neq)	5.28	5.35	5.15	5.38
osc st (neq)	0.00	0.25	0.00	0.26

eV. However, extension of the basis set size and inclusion of solute–solvent hydrogen bonding interactions decrease the relative stability of  $T_n$ ,<sup>34,35</sup> making it less stable by  $\sim 0.3\text{ eV}$  than  $T_\pi$  for isolated T. Because  $T_n$  is not affected by stacking interactions, this value is a lower bound to the energy difference within a single strand, as confirmed by test calculations on a TpT model (see Figure 1) explicitly including eight water molecules (see below).

Test PCM/M052X/6-31G(d) calculations on  $\text{TMP-H}^-$  indicate that C2-endo conformer is more stable than C3-endo by  $\sim 1.3\text{ kcal/mol}$ , in agreement with the NMR experiments on TpT dinucleotides, indicating a C3/C2 ratio of  $\sim 0.35$ .<sup>15</sup> PCM/M052X/6-31G(d) calculations overestimate the  $S_0 \rightarrow T_\pi$  transition energy in the mononucleotide by  $\sim 0.7\text{ eV}$  (the experimental absorption maximum is  $\sim 4.65\text{ eV}$ ). The discrepancy with experiments would be much smaller using a larger basis set, including explicit water molecules<sup>34</sup> and considering the effect of the vibrations on the spectrum.<sup>68</sup> Test calculations on thymine in the gas phase (Table 1 in the Supporting Information), show indeed that the M052X results are very close to those obtained by using CASPT2,<sup>69</sup> CC2,<sup>69</sup> and CCSD(T) calculations,<sup>70</sup> being less than 0.2 eV blue-shifted with respect to the CCSD(T) estimate (by comparison CC2 exhibits a larger blue shift).

For the purposes of the present study it is, however, more important to verify the effect of the stacking on the excited state properties than to reproduce the absolute absorption maxima; we shall thus mainly exploit the smaller 6-31G(d) basis set, allowing a more complete exploration of the conformational space. To make easier the comparison with the experimental results, in the following we shall also report corrected absorption ( $\nu_A$ ) and emission ( $\nu_E$ ) energies, labeled by a superscript c ( $\nu_A^c$  and  $\nu_E^c$ ,  $\lambda_A^c$  and  $\lambda_E^c$  on a wavelength scale), scaled by 0.7 eV.

**3.1.2. TpT Deoxy-Dinucleotide.** We have optimized in water the geometry of five different conformers of TpT, differing for the conformations of the furanose ring and, therefore, for the backbone parameters (Table 2, Figure 2, and Supporting Information): TpT-c3c3, TpT-c2c2, TpT-c3c2, TpT-c2c3, and TpT-c2c1.

**Table 2.** Main Structural Features of Different Conformers of TpT in Aqueous Solution According to PCM/M052X/6-31G(d) Geometry Optimizations (Relative Energies in kcal/mol)

	TpT-c3c3	TpT-c2c2	TpT-c2c1	TpT-c3c2	TpT-c2c3
$\delta$ (deg)	86.5	143.0	144.6	88.1	142.6
$\epsilon$ (deg)	-120.0	178.0	-168.8	-129.9	-178.0
$\zeta$ (deg)	-64.0	-101	-84.6	-67.0	-105.2
$\alpha$ (deg)	-65.0	-61.0	-63.2	-57.1	-67.6
$\beta$ (deg)	165.0	-176.0	170.4	170.3	170.8
$\gamma$ (deg)	56.0	55.0	55.4	62.0	56.2
$\chi$ (deg)	-172.0	-123.0	-121.0	-172.0	-123.9
$\nu_0$ (deg)	10.0	-16.6	-24.0	8.2	-16.6
$\nu_1$ (deg)	-29.7	30.5	36.1	-26.9	30.1
$\nu_3$ (deg)	-31.8	23.0	20.5	-30.2	22.2
$\nu_4$ (deg)	14.0	-4.2	2.1	14.1	-3.6
$\chi'$ (deg)	-157.0	-105.0	-102.0	-119.7	-136.7
$\nu_0'$ (deg)	3.1	-25.0	-39.0	-19.3	-2.2
$\nu_1'$ (deg)	-25.7	36.8	43.23	34.2	-20.1
$\nu_3'$ (deg)	-35.6	20.8	9.0	25.2	-35.1
$\nu_4'$ (deg)	20.9	2.4	18.7	-3.8	24.0
C5–C5' (Å)	3.6	4.6	3.8	3.7	5.2
C6–C6' (Å)	4.0	4.8	4.1	4.2	5.1
$d$ (Å)	3.7	4.7	3.9	3.9	5.1
C5–O8' (Å)	3.6	4.3	3.5	3.4	4.7
C5'–O8 (Å)	4.3	5.1	4.7	4.4	5.8
$\eta$ (deg)	54.4	37.0	51.4	55.7	49.6
energy <sup>a</sup>	0	2.4	3.9	0.4	2.6
energy <sup>b</sup>	0	1.7	5.0	0.06	1.9

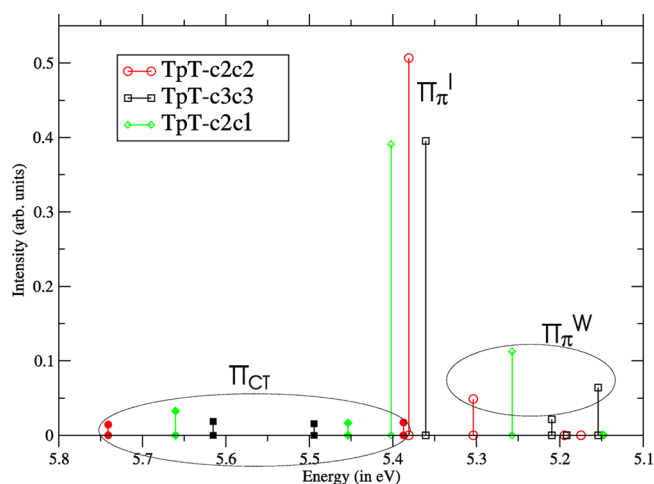
<sup>a</sup>6-31G(d) results. <sup>b</sup>6-31+G(d,p) results.

PCM/M052X calculations predict that TpT-c3c3 is the most stable conformer, being  $\sim 2$  kcal/mol more stable than TpT-c2c2. Actually, methoxy TpT derivatives,<sup>15</sup> preferring a C3 endo pucker of the sugar, exhibit a 3 times higher fraction of stacked conformer than TpT. This finding suggests that C3 puckering favors T stacking, and conversely, for stacked conformers, as those we examine, C3 puckering should be relatively more stable than C2 puckering. In any case, an accurate characterization of the conformational equilibrium in TpT (by no means a trivial task)<sup>67</sup> is outside the scope of the present paper, focusing “simply” on the dependence of TpT photochemical behavior on the strand conformation.

As shown in Table 2 and in Figure 2, the stacking geometries of the conformers examined are significantly different. TpT-c3c3 exhibits a tighter stacking geometry than the other

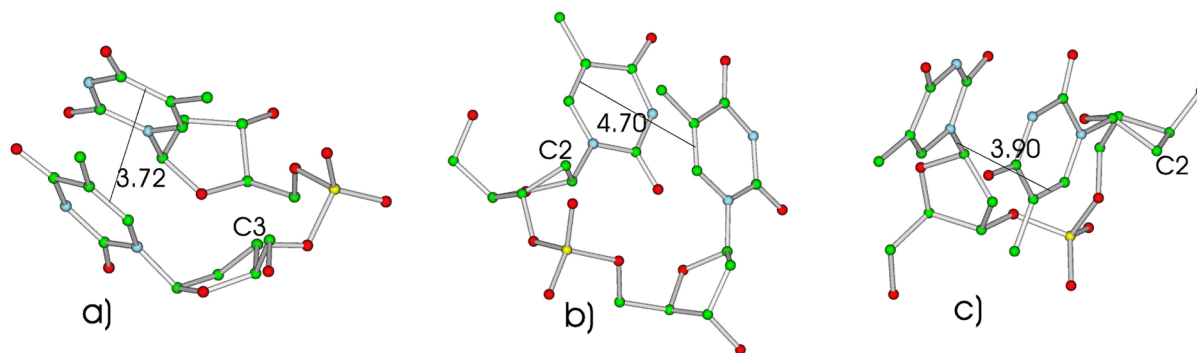
conformers: the distance ( $d$ ) between the “center” of the C5C6 double bonds of the two monomer is  $\sim 3.7$  Å and the C5–C5' distance is only 3.56 Å. Just to make an example, for TpT-c2c2  $d$  is 4.7 Å and the C5C5' distance is 4.6 Å. Inclusion of the counterion does not lead to significant differences in the structural properties of the different conformers and in their relative energy (Table 1 in the Supporting Information).

**3.1.2.a. Absorption Spectra.** The absorption spectra of TpT conformers are reported in Figure 3 and Table 3.

**Figure 3.** Stick absorption spectra computed in water for three conformers of TpT at the LR-PCM/M052X/6-31G(d) level. The energy of the electronic transition with significant CT character has been corrected on the ground of SS-PCM calculations.

Independently of the backbone conformation, we obtain a qualitatively similar picture. The four lowest energy excited states are reminiscent of the monomer  $T_\pi$  and  $T_n$  states. We indeed find two  $T_n$ -like  $n\pi^*$  electronic transitions localized on the two T moieties (hereafter  $T_n$  and  $T'_n$ ), with a transition energy very close to that of their counterpart in TMP. Due to the electronic coupling, the two bright transitions are no more degenerate and exhibit different intensities: one, on the blue side, is bright and intense ( $TT_\pi^I$ ), and the other one, on the red wing, is weaker ( $TT_\pi^W$ ). The frontier orbitals and the corresponding bright electronic transitions are delocalized over the two bases of TpT.

The electronic coupling is rather small. Indeed,  $TT_\pi^I$  is very close in energy to the  $T_\pi$  transition in the monomer, whereas  $TT_\pi^W$  is red-shifted by  $\sim 0.1$ – $0.25$  eV. These estimates are fully

**Figure 2.** Schematic drawing of three of the 5 TpT conformers investigated in the present study: (a) TpT-c3c3; (b) TpT-c2c2; (c) TpT-c2c1. TpT-c2c3 and TpT-c3c2 structures are depicted in the Supporting Information.

**Table 3. Energy (in eV) and Oscillator Strength (in parentheses) of the Five Lowest Energy Excited States of TpT. LR-PCM/TD-M052X/6-31G(d) Calculations in Aqueous Solution**

	TpT-c3c3	TpT-c2c2	TpT-c2c2-8H <sub>2</sub> O	TpT-c2c1	TpT-c3c2	TpT-c2c3	TpT <sub>I</sub>
TT <sub>π</sub> <sup>W</sup>	5.15(0.06)	5.30(0.05)	5.21(0.04)	5.26(0.11)	5.22(0.05)	5.29(0.12)	5.12(0.05)
TT <sub>π</sub> <sup>I</sup>	5.36(0.40)	5.38(0.51)	5.32(0.52)	5.40(0.39)	5.37(0.41)	5.37(0.41)	5.40(0.44)
TT <sub>CT</sub>	5.89(0.01)	6.10(0.01)	5.90(0.01)	5.98(0.03)	5.99(0.01)	6.35(0.00)	5.93(0.01)
T <sub>n</sub>	5.19(0.00)	5.17(0.00)	5.46(0.00)	5.15(0.00)	5.14(0.00)	5.21(0.00)	5.16(0.0)
T' <sub>n</sub>	5.21(0.02)	5.19(0.00)	5.56(0.00)	5.15(0.00)	5.19(0.03)	5.22(0.00)	5.18(0.02)

consistent with those obtained at the MCSCF level by Serrano-Perez et al., which predict the lowest energy transition in the stacked dimer is 0.29 eV red-shifted with respect to the isolated monomer.<sup>25</sup>

The electronic coupling between the monomers and, therefore, the position of the lowest energy  $\pi\pi^*$  state significantly depend on the conformation, being the largest for TpT-c3c3, which exhibits the smallest  $d$  value. In TpT-c3c3, TT<sub>π</sub><sup>W</sup> is indeed red-shifted by  $\sim 0.25$  eV with respect to T<sub>n</sub>, whereas for TpT-c2c2 the red-shift is just  $\sim 0.1$  eV. A more parallel arrangement (smaller values of  $\eta$  dihedral angle) would also increase the coupling, but our calculations do not provide meaningful insights on this issue, because the conformers exhibit  $\eta$  values in a rather narrow range (between 35° and 50°) and, furthermore, those with the smallest  $\eta$  (TpT-c2c2) are also those with a much larger stacking distance.

LR-PCM/M052X-631G(d) calculations predict that the lowest energy transition with substantial T  $\rightarrow$  T CT character (TT<sub>CT</sub>, corresponding to S<sub>5</sub>) is ca. 0.6 eV blue-shifted with respect to TT<sub>π</sub><sup>I</sup>. On the other hand, LR-PCM calculations underestimate the stability of CT states, whose treatment requires SS-PCM calculations.<sup>40,41,57</sup> SS-PCM/M052X/6-31G(d) calculations (Table 4) predict indeed that the relative stability of the lowest energy CT state is  $\sim 0.3$ – $0.4$  eV larger than at the LR-PCM level. Because “neutral” excited states such as TT<sub>π</sub><sup>I</sup> and TT<sub>π</sub><sup>W</sup> are confirmed to be reliably described already by LR-PCM/TD-DFT calculations,<sup>41</sup> at the SS-PCM level, TT'<sub>CT</sub> is, on average, slightly on the blue of the absorption band maxima. Due to the asymmetry of the stacking geometry the two possible TT<sub>CT</sub> transition, i.e., T<sup>+</sup>  $\rightarrow$  T'<sup>-</sup> (5'T<sup>+</sup> and 3'T<sup>-</sup>, hereafter labeled as TT'<sub>CT</sub>) and T'<sup>+</sup>  $\rightarrow$  T<sup>-</sup> (5'T<sup>-</sup> and 3'T<sup>+</sup>, hereafter labeled as T'T<sub>CT</sub>) are not isoenergetic and, interestingly, their relative energy ordering depends on the backbone conformation. In fact, for TpT-c2c2, TT'<sub>CT</sub> is more stable than T'T<sub>CT</sub> by  $\sim 0.35$  eV, whereas for TpT-c2c1 it is less stable by  $\sim 0.2$  eV. Conformation significantly affects the relative stability of TT<sub>π</sub><sup>W</sup> and TT'<sub>CT</sub>: for TpT-c2c2, these two transitions are very close in energy (within 0.1 eV); for TpT-c3c3, TT<sub>π</sub><sup>W</sup> is 0.35 eV more stable than TT'<sub>CT</sub>.

The picture obtained for TpTNa (Table 2 in the Supporting Information) is very similar to that just described. SS-PCM test calculations on TpTNa-c2c2 indicate that TT'<sub>CT</sub> is  $\sim 0.1$  eV less stable than TT<sub>π</sub><sup>I</sup> whereas in the absence of the Na counterion, it is  $\sim 0.03$  eV more stable. This result confirms that the energy of the CT excited state is significantly modulated by the fluctuation of the charged moieties of the backbone (see below). On the other hand, inclusion of the counterion does not qualitatively affect our conclusions.

To better compare the computed absorption spectra with their experimental counterpart, we have convoluted each transition with a phenomenological Gaussian, by using the procedure described in the previous section (Figure 4). When compared with the spectrum of the monomer, a small

**Table 4. Main Features of the Lowest Energy Exciton and CT States of the Different Conformers of TpT in Aqueous Solution According to SS-PCM/TD-M052X/6-31G(d) Calculations on PCM/M052X/6-31G(d) Optimized Geometries (Nonequilibrium Solvation Using Gaussian03 Defaults;  $\nu_A$ , eV)**

state <sup>a</sup>	TT <sub>π</sub> <sup>W</sup>	TT <sub>π</sub> <sup>I</sup>	TT'-CT	T'T <sub>CT</sub>
TpT-c3c3				
$\nu_A$ (neq)	5.15	5.37	5.49	5.62
$\nu_A$ (eq)	to Sn	5.35	4.41	4.39
osc st (au)	0.06	0.31	0.015	0.02
Q <sub>m</sub>				
T <sub>1</sub>	-0.01	-0.01	0.68	-0.67
T <sub>2</sub>	0.01	0.01	-0.69	0.63
$\nu_m$				
T <sub>1</sub>	0.29	0.21	0.68	0.72
T <sub>2</sub>	0.15	0.21	0.74	0.63
TpT-c2c2				
$\nu_A$ (neq)	5.31	5.42	5.39	5.75
$\nu_A$ (eq)	5.27	5.38	3.63	4.02
osc st (au)	0.04	0.41	0.02	0.01
Q <sub>m</sub>				
T <sub>1</sub>	-0.01	-0.03	0.68	-0.78
T <sub>2</sub>	-0.01	0.00	-0.71	0.77
$\nu_m$				
T <sub>1</sub>	0.13	0.28	0.68	0.88
T <sub>2</sub>	0.29	0.14	0.78	0.77
TpT-c2c1				
$\nu_A$ (neq)	5.31	5.44	5.66	5.45
$\nu_A$ (eq)	5.28	5.40	4.18	4.08
osc st (au)	0.09	0.32	0.02	0.02
Q <sub>m</sub>				
T <sub>1</sub>	-0.01	0.00	0.67	-0.76
T <sub>2</sub>	-0.02	-0.03	-0.70	0.75
$\nu_m$				
T <sub>1</sub>	0.33	0.12	0.67	0.83
T <sub>2</sub>	0.11	0.30	0.79	0.85

<sup>a</sup>T<sub>1</sub> and T<sub>2</sub> refer to the two thymine of TpT.

hypochromic shift is found (10/25% depending on the backbone conformation), fully consistent with the experiments on (dT)<sub>20</sub><sup>31</sup> (hypochromic shift of 12%). Furthermore, the presence of a red tail is predicted, in agreement with experimental results on (dT)<sub>20</sub>,<sup>22,31</sup> which is due to two different factors. The first is the contribution of TpT-c3c3 that exhibits a much larger absorption intensity for  $\nu_A$  in the range 5.1–4.6 eV ( $\nu_A^c$  4.4–3.9 eV,  $\lambda^c$  280–320 nm), essentially due to the red-shifted position of TT<sub>π</sub><sup>W</sup>. The second is the contribution of TT<sub>CT</sub> transitions, due to their very large inhomogeneous broadening, being responsible of the absorption for  $\lambda^c > 320$  nm (see the spectrum of the TpT-c3c3 conformer in Figure 5 and that of TpT-c2c2<sup>31</sup> in Figure 2 of the Supporting

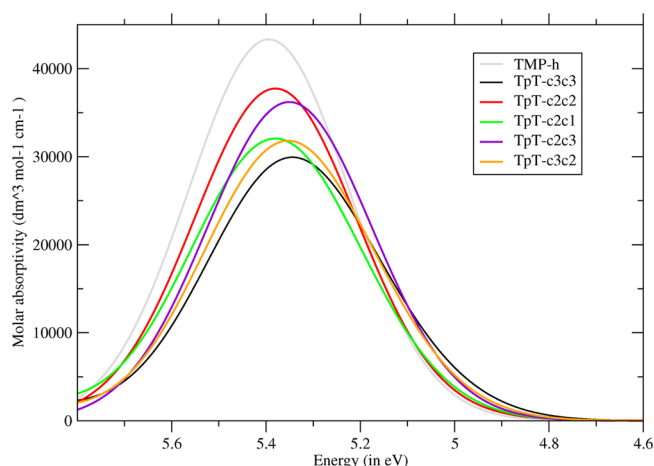


**Figure 4.** Absorption spectra computed in water for five conformers of TpT convoluting each transition by a Gaussian with fwhm 0.2 eV.

Information). For this latter conformer, the red wing (up to  $\nu_A^c$  3.5 eV, i.e.,  $\lambda^c$  350 nm) is indeed due to the CT transitions. The weak blue shift of the absorption maximum<sup>31</sup> is not reproduced; however, it is sufficient to increase the basis set size at the 6-31+G(d,p) level and also this experimental finding is recovered (see Supporting Information).

Finally, test calculations on a model including eight water molecules (Table 3 and Supporting Information) show that  $TT_\pi$  bright excited states experience a weak red shift, whereas  $n\pi^*$  transitions have a significant blue shift. As a consequence, the stability order predicted without explicitly including solute–solvent hydrogen bonds is reversed,  $T_n$  and  $T'_n$  being  $\sim 0.3$  eV less stable than  $TT_\pi^W$ .

**3.1.2.b. ECD Spectra.** Figure 6 reports the ECD spectra computed for the different TpT conformers. The shape of the spectra is in very good agreement with its experimental counterpart, predicting a strongly positive feature on the red wing (at  $\sim 275$  nm), followed by a negative one, with similar height,  $\sim 0.35$  eV on the blue (at  $\sim 255$  nm).<sup>4,13</sup> This result is extremely similar to the prediction of our calculations, especially for the TpT-c3c3 conformer, that exhibiting the

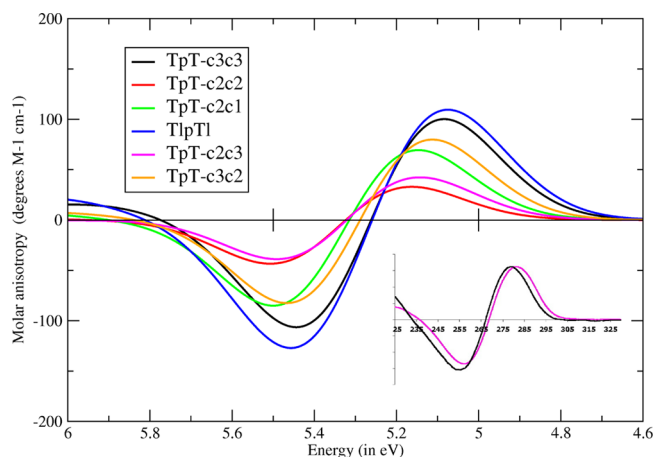


**Figure 6.** ECD spectra computed in water for five conformers of TpT and for TpT<sub>1</sub> at the LR-PCM/M052X/6-31G(d) level, convoluting each transition by a Gaussian with fwhm 0.2 eV.

most intense ECD spectrum (and that should be the predominant stacked conformer). The good agreement with the experimental ECD spectrum confirms that our calculations are able to reproduce the effect of the stacking on the TpT electronic transitions, not only qualitatively but also quantitatively. In this respect, the energy shift between  $TT_\pi^W$  (responsible of the positive feature) and  $TT_\pi^I$  (main responsible of the negative one) is correctly estimated. Not surprisingly, the intensity of the spectrum is overestimated with respect to the experimental one, because unstacked conformers, not significantly contributing to the ECD spectrum, are also present in solution. The intensity computed for TpT-c3c3 is  $\sim 8$  times larger than the experimental one, suggesting that  $\sim 12\%$  of TpT is stacked in solution. On the other hand, this can be considered only a very rough estimate. Besides the intrinsic limitations of our computational model (functional, basis sets, absence of explicit water molecules), the computed intensity for all the other conformers (which could also contribute to the total spectrum) is much lower than that found for TpT-c3c3. Furthermore, because the ECD spectrum is sensitive to the stacking geometry, a single minimum (though representative)

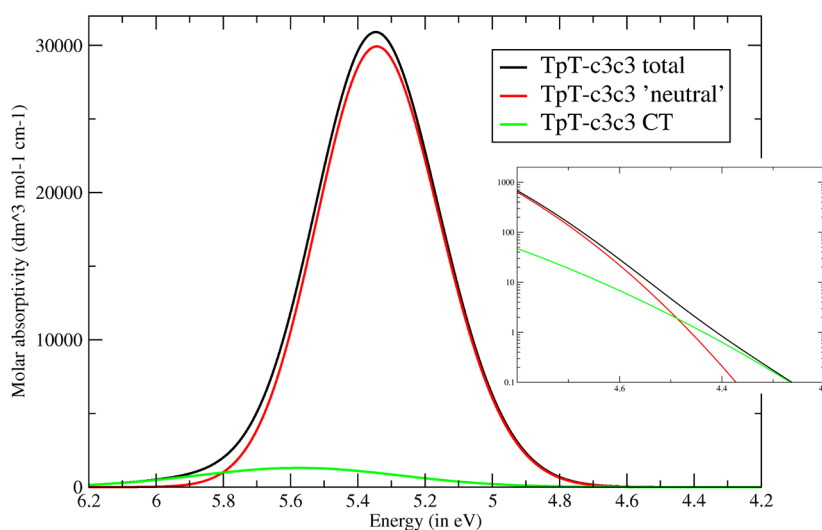


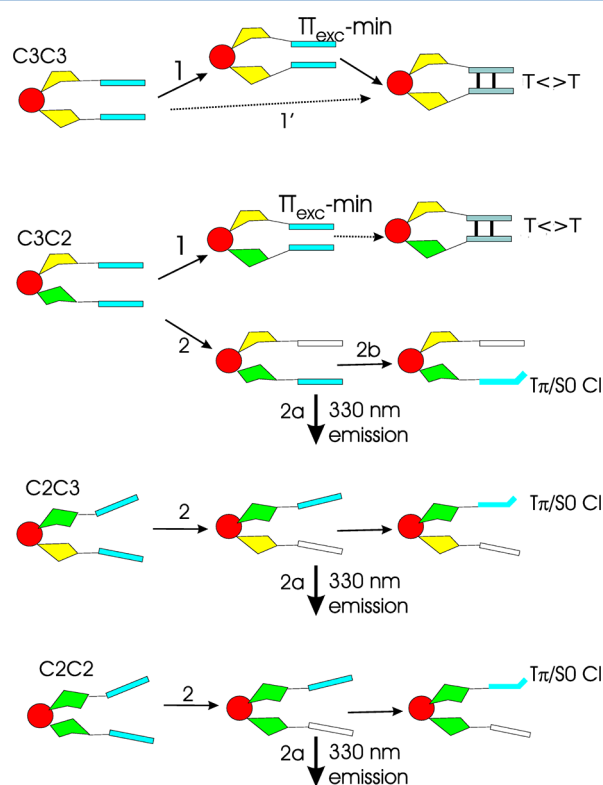
**Figure 5.** Absorption spectra computed in water for TpT-c3c3 conformer convoluting each transition by a Gaussian with fwhm = 0.2 eV for “neutral” transitions and fwhm = 0.35 eV for CT transitions. A close-up of the red-wing is also shown.



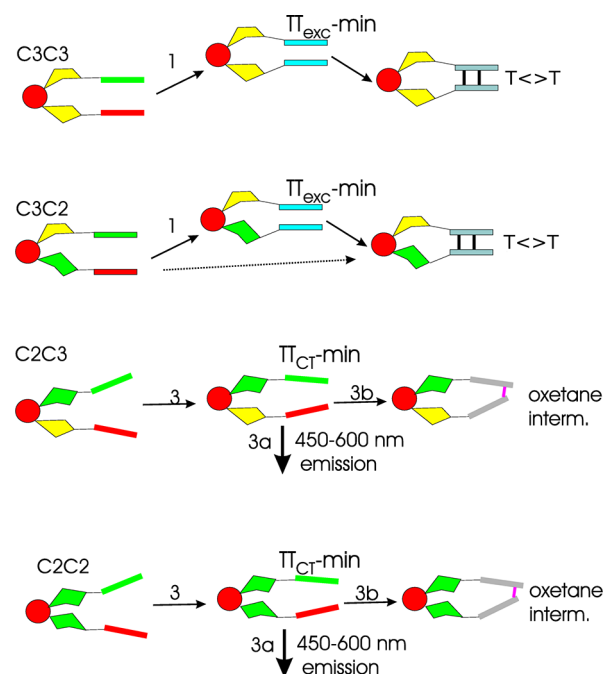
cannot fully reproduce the effect of the complex conformational behavior occurring in solution.

**3.1.3.  $T_pT_l$  Locked Dinucleotide.** The  $S_0$  optimized geometry of  $T_pT_l$ , adopting a C3–C3' endo pucker, is rather similar to that of  $TpT$ -c3c3, with a smaller stacking distance: the C5–C5' distance is 3.46 Å and the C6–C6' distance 3.82 Å. The computed absorption spectra of  $T_pT_l$  and  $TpT$ -c3c3 are also similar (see the last column of Table 3) with a slightly larger energy separation between  $TT_\pi^w$  and  $TT_\pi^l$  for  $T_pT_l$ , indicating that the closer approach between the two bases increases electronic coupling. The computed ECD spectrum (Figure 6) is also in very good agreement with its experimental counterpart. In particular, our calculations reproduce the weak red shift of the positive peak, which is due to the red shift of  $TT_\pi^w$  in  $T_pT_l$ . Also in this case the intensity of the spectrum is larger than the experimental one, but the ratio is in this case smaller ( $\sim 3$ ), indicating that a larger fraction of  $T_pT_l$  in solution is stacked, in line with the indication of experiments and MD simulations.<sup>19</sup>

**3.2. Excited State Deactivation Paths.** In the following we report a general description of the main excited state decay paths of  $TpT$  and  $TpTNa$ . As detailed below and schematically depicted in Figures 7 and 8, for the bright excited states the most relevant pathways are (i) the formation of  $T<>T$ , in some case passing through an excimer minimum (path 1 and 1' in Figure 7) and (ii) the localization of the excitation (path 2 in Figure 7) on a single monomer then following the same decay routes of isolated  $T$ . CT states decay to a minimum (path 3 in



**Figure 7.** Schematic drawing of the main decay routes of the bright excited states in  $(dT)_2$  single strands. Each bar schematically represents a Thy base, and the intensity of the color is proportional to the participation of the base in the electronic transition. For simplicity, only one of the monomer-like decay paths possible for  $TpT$ -c2c3 and  $TpT$ -c2c2 is shown.



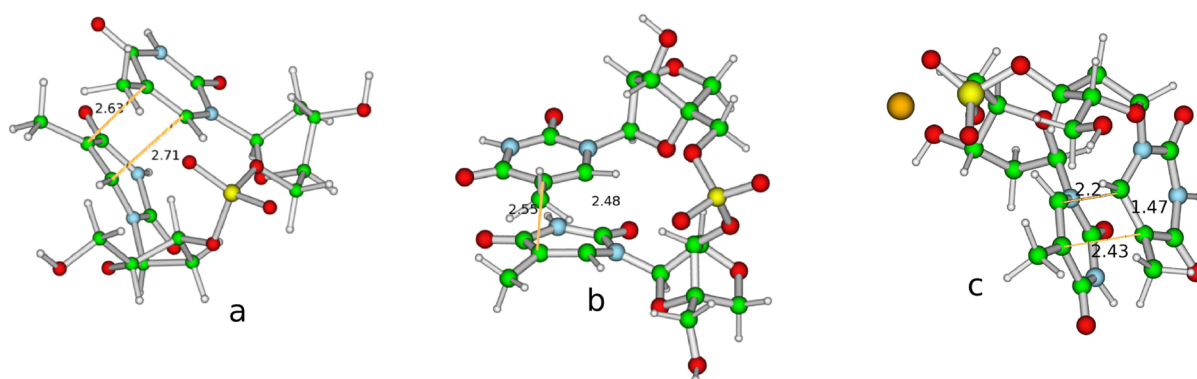
**Figure 8.** Schematic drawing of the main decay routes of the  $TT'$  CT excited state in  $(dT)_2$  single strands. Each bar schematically represents a  $T$  base.  $T^+$  and  $T^-$  bases are depicted in green and in red, respectively.

Figure 8) that (path 3b in Figure 8) can lead to the formation of oxet. The fate of the reaction is modulated by the backbone conformation. A detailed description of the results obtained for the different conformers can be found in the Supporting Information.

**3.2.1. Bright Excited States.** **3.2.1.a. Decay to Excimer Minimum and  $T<>T$  Formation.** PCM/TD-M052X/6-31G(d) geometry optimizations predict that  $TT_\pi^w$  (for  $TpT$ -c3c3 and  $TpT$ -c3c2) and  $TT_\pi^l$  (for  $TpT$ -c3c3, see Supporting Information for details) decay to an excimer minimum ( $TT_{exc-min}$ ), whose main features do not significantly depend on the backbone conformation. In the following our discussion will be based on the minimum found for  $TpT$ -c3c3 (Figure 9). The excitation is delocalized over the two  $T$  monomers, although not symmetrically, as shown by the different values of C5C6 (1.43 Å) and C5'C6' (1.40 Å) bond distances, and the stacking distances between the two carbon double bonds is rather small (C5C5' = 2.63 Å; C6C6' = 2.71 Å; C6C5' = 2.78 Å). The computed  $\nu_E$  from  $TT_{exc-min}$  (SS-PCM/TD-M052X/6-31G(d) calculations) is 2.61 eV, with a very weak intensity (oscillator strength 0.01). Geometry optimizations using a larger 6-31+G(d,p) basis set provide similar indications, predicting the presence of excimer minimum characterized by rather short C5–C5' and C6–C6' distances ( $\sim 2.7$ – $2.8$  Å). This picture does not change when the M062X functional is used and when the  $Na^+$  counterion is included in our model.

To further analyze the reactivity of  $TT_{exc-min}$ , we have performed a minimum energy path (MEP) for different values of the C6–C6' distance (Figure S4 in the Supporting Information). As detailed in the Supporting Information, a very small energy barrier (upper bound 0.03 eV) separates  $TT_{exc-min}$  from the crossing region with  $S_0$ , characterized by very small distances between the C5C6 and C5'C6' bonds and long C5C6 and C5C6' bond distance. A representative structure of the crossing region (C6–C6' distance = 2.2 Å,





**Figure 9.** Schematic drawing of the excimer minimum found for (a) TpT-c3c3 and (b) for TpT<sub>T</sub> by LR-PCM/TD-M052X/6-31G(d) calculations; (c) a representative point of the S<sub>1</sub>/S<sub>0</sub> crossing region in the T<>T path found for TpTNa-c3c3 (TpT<sub>T<>T</sub>-CI\*).

S<sub>0</sub>/S<sub>1</sub> energy gap 0.4 eV) is shown in Figure 9. It is similar to the CI found for the isolated T dimer in the T<>T reactive path, and thus representative of the crossing region in the path leading to T<>T formation (TpT<sub>T<>T</sub>-CI\*) for TpT.

The estimated value of the energy barrier separating TT<sub>exc</sub>-min and TpT<sub>T<>T</sub>-CI\* is well below the expected accuracy of our calculations and the barrier height is an upper bound to the real value, because the transition state has not been located. Taking into account the kinetic energy (up to ~0.5 eV) of the system when reaching TT<sub>exc</sub>-min, and the possible effect of thermal fluctuations, the decay to TpT<sub>T<>T</sub>-CI\* can be considered barrierless. As a matter of fact, for TpT-c2c1 (also when including Na<sup>+</sup> counterion) geometry optimization does not find any minimum on the TT<sub>π</sub><sup>I</sup> excited state PES: the C6–C6' distance decreases until a crossing region with S<sub>0</sub> is found,<sup>31</sup> very similar to TpT<sub>T<>T</sub>-CI\* and corresponding to the CI in the path leading to T<>T formation.<sup>31</sup>

**3.2.1.b. Monomer-Like Decay Paths.** For TpT-c2c2 and TpT-c2c3 PCM/TD-M052X/6-31G(d), geometry optimizations of both TT<sub>π</sub><sup>W</sup> and TT<sub>π</sub><sup>I</sup> indicate localization of the excitation on a single T monomer (T<sub>π</sub>) excited state, TT<sub>π</sub><sup>W</sup> decaying to T'π (localization on the 3' T), whereas TT<sub>π</sub><sup>I</sup> decays to T<sub>π</sub> (localization on the 5' T). Analogously TT<sub>π</sub><sup>I</sup> of TpT-c3c2 and TT<sub>π</sub><sup>W</sup> of TpT-c3c1 decay to T<sub>π</sub> (path 2 in Figure 7). The system then follows the same decay pathway of an isolated T base.<sup>38</sup> Just to make an example, geometry optimization of T'π in TpT-c2c2 shows a substantial lengthening (~0.1 Å) of the C5'–C6' bond, while the pyrimidine ring keeps an almost planar geometry. ν<sub>E</sub> from a representative structure (T'π-pla) from this energy plateau (energy gradient ~0.002 au) is 4.50 eV, with a rather high oscillator strength (0.18). ν<sub>E</sub><sup>E</sup> is thus 3.80 eV (λ<sub>E</sub><sup>C</sup> = 330 nm): “monomer-like” emission from T'π-pla (path 2a in Figure 7) could thus contribute, together with fluorescence of completely unstacked bases, to the maximum of the emission band measured for (dT)<sub>20</sub>.<sup>31</sup> Geometry optimization then provides disruption of the planarity of the pyrimidine ring, adopting a “bent” geometry and moving in a nonplanar energy plateau. ν<sub>E</sub> of a representative point of this plateau, T'π-bent (Figure 10), is 3.64 eV with an oscillator strength of 0.12. T'π-bent is only 0.11 eV more stable than T'π-pla and it is connected by a steep and barrierless path, involving strong C5' pyramidalization and out-of-plane motion of the methyl group, to a CI with S<sub>0</sub> (Figure 10) T'π-CI, where the T'π/S<sub>0</sub> energy gap is <0.1 eV. Within TpT the system can thus follow the same decay path of isolated T (path 2b in Figure 7).

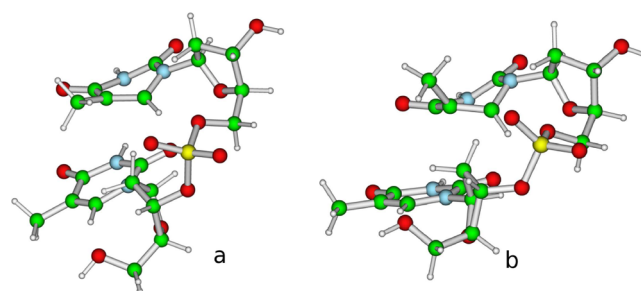


**Figure 10.** Schematic drawing of the two representative points of the “monomer-like” path found for TpT-c2c2 by LR-PCM/TD-M052X/6-31G(d) calculations: (a) nonplanar plateau (T'π-bent); (b) conical intersection with S<sub>0</sub>.

**3.2.2. Dark Excited States. 3.2.2.a. nπ\* Excited States.** For all the conformers examined, geometry optimizations of the T<sub>n</sub> and T'<sub>n</sub> lead to the minimum already described for the nπ\* excited state in isolated T,<sup>38,39</sup> where the pyrimidine ring keeps a planar geometry and the C4O8 distance increases up to 1.31 Å. The only difference with respect to previous computational studies is that, according to PCM/TD-M052X, the C4O8 carbonyl group undergoes a small partial pyramidalization and it is no longer coplanar with the molecular ring (Figure 6 in the Supporting Information), likely due to the formation of a weak hydrogen bond with the adjacent base. No sign of photochemical reactivity of T<sub>n</sub> states is found, excluding<sup>31</sup> any significant involvement in the T<>T or in 6-4TT formation.<sup>16</sup>

**3.2.2.b. CT Excited States.** LR-PCM/TD-M052X/6-31G(d) optimizations of the CT states predict a sudden decay to a TT<sub>π</sub> exciton. This result is not surprising, because LR-PCM calculations underestimate the stability of the CT states. Unfortunately, excited geometry optimizations at the SS-PCM level are not feasible. As a consequence, to get an estimate of the structural features of TT<sub>CT</sub> states minima, we performed LR-PCM/PBE0 geometry optimizations, exploiting that the overestimation of the CT stability by PBE0 makes geometry optimizations less cumbersome, then refining the PBE0 minima at the M052X level.

PCM/TD-PBE0/6-31G(d) geometry optimizations of TT'<sub>CT</sub> and T'T<sub>CT</sub> predict that, independently of the backbone conformation, the most significant geometry shifts involve the intramonomer degrees of freedom, the two bases adopting the geometry of T<sup>+</sup> cation and T<sup>−</sup> anion respectively. Geometry optimizations of T'T<sub>CT</sub> (5'T<sup>−</sup> and 3'T<sup>+</sup>) then predict, for all the conformers, a very close approach of the O8 atom (bearing

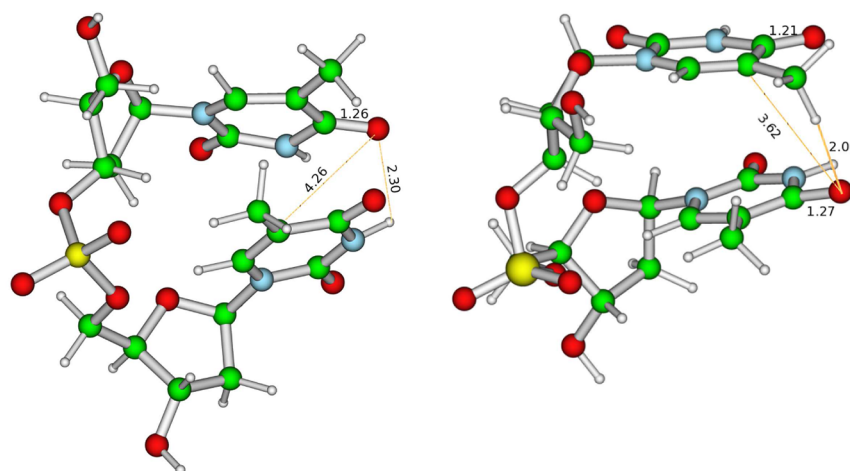


**Figure 11.** Schematic drawing of (left) the pseudominima of the  $T'T_{CT}$  state and (right) of the  $TT'_{CT}$  predicted by LR-PCM/PBE0/6-31G(d) calculations for TpT-c3c3.

an excess of negative charge) to the N3'-H group, providing the formation of a strong hydrogen bond (O8-H distance  $\sim 2.1$  Å, Figure 11), followed by a barrierless proton transfer reaction. Refining the PBE0 optimizations by M052X calculations, however, shows that CT states are mixed with bright excited states and, indeed, LR-PCM/M052X/6-31G(d) geometry optimization provides the decay of  $T'T_{CT}$  to the excimer minimum  $TT_{exc-min}$  (see Supporting Information for details).

For  $TT'_{CT}$  ( $5'T^+$  and  $3'T^-$ ), the O8' atom approaches the C5-CH<sub>3</sub> group, and then the fate of this process strongly depends on the backbone conformation. Indeed, for TpT-c3c3, TpT-c3c2, and TpT-c2c1 the O8' atom forms a hydrogen bond with one of hydrogen atoms of the methyl group (Figure 11). However, this minimum decays to  $TT_{exc-min}$  (for TpT-c3c3 and TpT-c3c2) or directly to  $TpT_{T \rightarrow T}CI^*$  (for TpT-c2c1) according to LR-PCM/M052X/6-31G(d) optimizations (Figure 8).

For TpT-c2c2 and TpT-c2c3 we obtain instead a very different picture: O8' atom approaches the C5 atom, as in a nucleophilic attack of the negative moiety toward the positive one, reaching a pseudominimum ( $TT'_{CT-min}^*$ , Figure 12) where the O8' atom of the  $3'T^-$  anion is very close to the C5 atom of the  $5'T^+$  cation. We analyze more in detail the minimum located for TpT-c2c3, starting from the dependence of the emission energy on environmental effects. In longer oligonucleotide chains, T residues are indeed less exposed to the solvent than in TpT, reducing the "effective" dielectric

constant experienced by  $TT'_{CT-min}$ . The emission energy of the CT state could also be sensitive to the presence of the counterions. To explore these possibilities, we have located  $TT'_{CT-min}^*$  also for TpTNa-c2c3 and computed the emission energy for two smaller dielectric constants ( $\epsilon = 78.4$  as in water,  $\epsilon = 8$  and  $\epsilon = 4$ ). For TpT-c2c3  $\nu_E$  from  $TT'_{CT-min}^*$ , computed at the SS-PCM/M052X/6-31G(d) level, are in the range 2.21 eV ( $\lambda_E = 560$  nm,  $\epsilon = 78.4$ ) to 3.03 eV ( $\lambda_E = 410$  nm,  $\epsilon = 4$ ). For TpTNa-c2c3, computed  $\nu_E$  are 2.26 eV ( $\epsilon = 78.4$ ), 2.61 eV ( $\epsilon = 8$ ), and 3.02 eV ( $\epsilon = 4$ ). Extension of the basis set does not affect significantly  $\nu_E$ : for TpT-c2c3, SS-PCM/TD-M052X/6-31+G(d,p) ( $\epsilon = 80$ ) provides a  $\nu_E$  value of 2.26 eV, i.e., slightly larger than that obtained at the 6-31G(d) level. These values are consistent with the position of the emission band recorded when (dT)<sub>20</sub> was excited in the UVA.<sup>31</sup> Although the contribution of the emission from bright exciton trapped in  $TT_{exc-min}$  is possible,  $TT'_{CT-min}^*$  is the more likely candidate for the red wing of the (dT)<sub>20</sub> emission band.

Both for TpT-c2c3 and TpT-c2c2, refinement of  $TT'_{CT-min}^*$  by LR-PCM/TD-M052X calculations leads indeed to a  $S_1/S_0$  crossing region (energy gap  $\sim 0.02$ – $0.2$  eV) with the TD-DFT calculations suffering from severe convergence problems (path 3b in Figure 8). A representative TpT-c2c3 structure of this region ( $TT_{oxet-CI}$ , see Supporting Information for TpT-c2c2) is shown in Figure 12: the O8' atom is very close to the C5 atom (distance  $\sim 1.58$  Å only) and the C4' atom is approaching the C6 atom (distance 2.40 Å), while both C5-C6 (1.42 Å) and C4'-O8' (1.31 Å) distances are approaching values typical of "standard" CC and CO single bonds, indicating that this is the crossing region in the path leading to the formation of oxet. We have analyzed more in detail the  $TT'_{CT-min}^* \rightarrow TT_{oxet-CI}$  path by using SS calculations, which are necessary for an accurate description of processes involving large variation of the electron density in polar solvents.<sup>57,71</sup> Also in this case, we have checked for the dependence of our estimate on the  $\epsilon$  used in the PCM calculations. At the solvent neq level this process is predicted to be slightly exoergic by  $-0.20$ – $-0.30$  eV (depending on the  $\epsilon$  used in the calculations). At the solvent eq level  $\Delta G$  associated with the  $TT'_{CT-min}^* \rightarrow TT_{oxet-CI}$  path is significantly endoergic, i.e.,  $\sim 0.80$  eV ( $\epsilon = 78.4$ ),  $\sim 0.5$  eV ( $\epsilon = 8$ ), and  $\sim 0.25$  eV ( $\epsilon = 4$ ). These can be considered only rough estimates, because only a more accurate

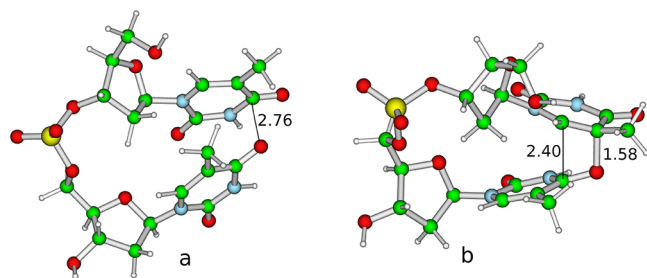


**Figure 12.** Schematic drawing of (left) the pseudominimum of the  $TT'_{CT}$  state (LR-PCM/PBE0/6-31G(d) calculations) and (right) a representative point of the  $TT'_{CT}/S_0$  crossing region in the path leading to the oxetane intermediate (LR-PCM/TD-M052X/6-31G(d) calculations) found for TpT-c2c3.

treatment, explicitly including the coupling between solute and solvent degrees of freedom, would be necessary for obtaining a fully reliable value, because we are also in the proximity of CI.<sup>72</sup> On the other hand, it is clear that a not-vanishing energy barrier is associated with the formation of oxet, confirming the preliminary results on TpT-c2c2.<sup>31</sup>

**3.2.3.  $T_pT_l$ .** Geometry optimization of  $TT_\pi^W$  indicates a steep decay to an excimer minimum ( $T_pT_l$ -exc-min, Figure 9), which, though similar to that found for TpT-c3c3, exhibits some structural differences. Indeed, the C5–C5' distance and C6–C6' distances are 0.1 Å shorter, and the  $\eta$  value smaller, indicating a larger similarity to the CI for the T<>T formation.  $\nu_E$  is indeed red-shifted with respect to that found in the excimer minimum of TpT-c3c3, being just  $\sim 2.12$  eV ( $\nu_E = 1.4$  eV). 6-31+G(d,p) geometry optimization also predicts the existence of the excimer minimum, with short C5C5' (2.59 Å) and C6C6 (2.53 Å) distances and  $\nu_E = 2.25$  eV.

Concerning CT states, LR-PCM/TD-PBE0/6-31G(d) geometry optimizations show that they are significantly mixed with the bright  $TT_\pi$  exciton states. Indeed,  $TT_{CT}$  has a less clear-cut CT character than that found for TpT-c3c3. Although the LUMO is mainly localized on the 5'-ter T and the HOMO on the 3'-ter T, this latter orbital receives a noticeable contribution from both monomers. A rather stable minimum is indeed found, in which the hydrogen bond O8–H–N3 is not so strong as found for TpT-c3c3. Refinement by PCM/M052X/6-31G(d) geometry optimizations, however, predicts the decay to  $T_pT_l$ -exc-min. Similar results are found for  $TT'_{CT}$ : a minimum close to the found for TpT-c3c3 decays to  $T_pT_l$ -exc-min at the PCM/TD-M052X level.

#### 4. DISCUSSION

We have reported a thorough study of the excited state behavior of TpT and TpTNa, focusing on some representative stacked conformers. Experiments on  $(dT)_{20}$  show indeed that the bright excited state decay of the unstacked molecules (the majority of the bases in oligo-Thy single strand) is very similar to that of isolated monomers.<sup>31</sup>

Our calculations indicate that, also in water and in the presence of the phosphoribose backbone, T<>T formation occurs from the  $\pi\pi^*$  bright singlet excited state, which in a stacked system gives rise to two delocalized excitons.<sup>23–25</sup> For these, excited state barrierless paths are found leading from the FC region to T<>T formation (paths 1 and 1' in Figure 7). When at least one of the sugar rings adopts a C3-endo puckering, the photoexcited systems can decay without any energy barrier to an exciton minimum ( $TT_{exc}$ -min). This decay pathway is particularly effective when both sugars have a C3-endo puckering. For  $T_pT_l$  the T<>T formation is therefore expected to be more favored than for TpT, in line with the experimental results: it is blocked in the C3endo–C3'endo conformation, favoring the stacking and decreasing the possibility of nonreactive stacking conformation, and  $TT_{exc}$ -min is closer to the  $S_1/S_0$  crossing region, as shown by the very low  $\nu_E$ . It is important to highlight, however, that T<>T formation is not limited to C3-endo/C3'-endo conformers, because we have shown that also for TpT-c2c1, when no sugar exhibits C3-endo puckering, a barrierless decay path to  $T_pT_{T<>T}$ -CI\* is found.<sup>31</sup> Our assignment is consistent with the very low dependence of the T<>T quantum yield on the excitation wavelength all over the main absorption band.<sup>31</sup> Indeed we have shown that both bright and weak excitons can decay to  $T_pT_{T<>T}$ -CI\*.

Interestingly, although TpT-c3c3 is the conformer with the shortest  $d$  distance, in the ground state minimum  $d$  is larger than the threshold value (3.52 Å) used to estimate the T<>T yield,<sup>20</sup> and decay to  $TT_{exc}$ -min and T<>T formation is predicted also for systems exhibiting even larger  $d$ . It is also true, however, that all the conformers exhibiting T<>T reactivity have, in the ground state,  $d < 3.95$  Å. In any case, the reason for the larger TT reactivity of C3endo–C3'endo can be traced in the large electronic coupling of this conformer, which is due to the whole stacking geometry and not only to  $d$ , leading to a very steep decay toward the region close to  $TT_{exc}$ -min and, then, to  $T_pT_{T<>T}$ -CI\*. The large coupling also disfavors the formation of  $TT_{CT}$  excited states, which, as discussed below, are the precursors of oxet and, therefore, of 6-4TT products. It is also possible that, within the single strand of a longer oligo-Thy chain, steric hindrances are larger than in TpT and the decay to  $T_pT_{T<>T}$ -CI\* more difficult, explaining that the computed “effective” threshold<sup>20</sup> is smaller than the  $d$  value in the conformer we have examined. In this respect, MD simulations on TpT dinucleotide predict, on the average, a larger  $d$  threshold than that found in  $(dT)_{18}$ .<sup>17</sup> Finally, concerning the dependence of T<>T formation on the  $\eta$  value, our calculations indicate that, although the motion from  $S_0$  minimum to  $T_pT_{T<>T}$ -CI\*, eventually through  $T_pT_{exc}$ -min, is obviously accompanied by a decrease of the  $\eta$  value, barrierless decay to T<>T is possible also starting from a geometry with a substantially high  $\eta$  value. For example, the  $\eta$  value in the  $S_0$  minimum of TpT-c2c1 is 51.4°.

Our calculations therefore show that solvent does not significantly affect the path leading to T<>T formation. This is not surprising because this reaction involves a neutral exciton without any significant CT character, with a small variation of the dipole moment with respect to the ground state and of the excited state density during the path. Due to its ultrafast T<>T formation, this reaction is not significantly affected by dynamical solvation effects.

Solvent significantly modulates, instead, the formation of oxet (path 3–3b in Figure 8), the likely intermediate for 6-4TT production. Our calculations indicate that the reactive excited states are  $TT_{CT}$  states or, more precisely,  $TT'_{CT}$  state, producing a  $T^+$  monomer in the 5' position and a  $T^-$  anion in the 3' position, whose relative stability in the FC region is much larger in a polar environment. Furthermore, a noticeable energy barrier, due to environmental dynamical effects, is associated with the  $TT'_{CT} \rightarrow TT_{oxet}$ -CI\* reaction. This picture is consistent with the wavelength dependence of the 6-4TT quantum yield, which is larger for short excitation wavelengths, where the absolute probability of populating the  $TT'_{CT}$  state is larger and the amount of energy provided to the system to overcome the excited state energy barrier is larger.<sup>31</sup>

The CT reactivity does not depend on the  $g$  value of the  $S_0$  minimum. Indeed, in the  $S_0$  minimum TpT-c3c3, which, according to our calculations, does not exhibit any oxet reactivity, has a much smaller  $g$  value than TpT-c2c2, which instead can decay to  $T_pT_{oxet}$ -CI\*. Critical factors are, instead, those affecting the probability of formation of  $TT'_{CT}$ . In this respect, short interatomic distances in the ground state minimum, especially for parallel arrangements, increase the exciton coupling, disfavoring the population transfer to  $TT'_{CT}$  from the bright exciton and favoring, conversely, the decay to bright exciton of the  $TT'_{CT}$  population. In this framework we can explain why, besides geometric considerations, the TpT-c3c3 conformer does not exhibit any measurable 6-4TT



quantum yield, as shown by the behavior of TpT locked analogues, for which the population of CT states is not favored. According to our calculations the oxet formation is favored for TpT-c2c2 and TpT-c2c3 conformers, those exhibiting the longest stacking distances. The possibility of populating  $TT'_{CT}$  therefore is not very sensitive to the stacking distance (obviously for not too distant T pairs) but to environmental effects such as dynamical solvent effects or backbone fluctuations. The same considerations apply to the reactivity of  $TT'_{CT}$ , which is influenced by the charge distribution of the T charged bases. For example, in the  $T^-$  anion a significant part of the excess charge ( $-0.2$  au) is located on O8, and in the  $T^+$  cation the  $C5-CH_3$  moiety bears an excess of positive charge. It is clear that the rate and yield of oxet formation will be affected, *inter alia*, by the location of the charged species of the phosphoribose backbone, modulating the height of the energy barrier in the path to  $TpT_{oxet}-CI^*$ . Finally, the directionality of the CT process, i.e., which between the 5' and the 3' monomer is negatively/positively charged, also matters. Backbone conformation can affect the relative stability of  $TT'_{CT}$  and  $T'T_{CT}$  states and, contemporarily, formation of the unreactive  $T'T_{CT}$  state could decrease the 6-4TT yield of potentially reactive conformations.

According our calculations, unreacted CT states, i.e., those not producing oxet intermediate, can follow different decay routes. They can radiatively decay to the ground state, being responsible for the long-living red-shifted emission revealed by time correlated single photon counting experiments,<sup>31</sup> or nonradiatively by charge recombination. Interconversion between CT and neutral exciton is also possible, explaining the low  $T<>T$  yield obtained also with excitation in the UVA (for  $\lambda > 300$  nm). The small amount of energy injected to the system is not sufficient to overcome the energy barrier in the path leading to  $TpT_{oxet}-CI^*$  but, once the system has decayed to  $TT_{exc}$  it can proceed along the barrierless path to  $T<>T$ . Interestingly, the interconversion between the  $\pi\pi^*$  exciton and CT states, through vibronic coupling, seems thus be a general feature of DNA excited state dynamics, because it has been proposed to be operative in both adenine<sup>40,73</sup> and cytosine dimers.<sup>74</sup>

Concerning the photophysical pathways, also stacked conformer monomer-like decay pathways (as paths 2 in Figure 7) are possible, but their relevance should be limited to more loosely stacked conformers (as TpT-c2c2 and TpT-c2c3). Localization of the excitation on a single T monomer in the  $\pi\pi^*$   $T_\pi$  state, followed by monomer-like decay to  $S_0$ , radiative (by emission at 330 nm) or nonradiative (via C5 pyramidalization and out-of-plane motion of the methyl substituent), is possible. On the other hand, it is likely that experiments are not able to find any spectral signature associated with this process, because it involves a small percentage of bases. Monomer-like behavior is dominated by unstacked or poorly stacked T, which represents the large majority of the bases. Furthermore, photochemical pathways represent important decay routes for the stacked molecules. As a consequence, the effect of the localization process on the fluorescence anisotropy should be negligible, as confirmed by the experiments.<sup>31</sup>

Our picture is based on the results obtained on TpT dinucleotide, and it is worth briefly discussing their relevance for interpreting the experimental results relative to other systems, as longer  $(dT)_n$  oligonucleotides or double strands. In this respect it is comforting that the  $T<>T$  yields found in TpT (1–2%) are similar to those found in longer strands such as

$(dT)_{18}$  ( $\sim 3\%$ ),<sup>4</sup> especially if considering that in  $(dT)_{18}$  each base has two possible “partners” for the dimerization. The similarity of the ECD spectra of TpT and  $(dT)_{18}$  also suggests that the main features of the bright excited states do not significantly depend on the chain length.<sup>4</sup> Analogously, the  $T<>T/6-4TT$  ratio is  $\sim 10$  both in TpT<sup>14</sup> and in  $dT_{20}$ ,<sup>20</sup> suggesting that the interplay between CT and “neutral exciton” should be similar in the two systems. In  $(dA)_{20}(dT)_{20}$  the order of magnitude of  $T<>T$  and 6-4TT photoproducts is the same as in  $(dT)_{20}$ , but the  $T<>T$  yield is smaller and the  $T<>T/6-4TT$  ratio larger.<sup>20</sup> This result suggests that the general mechanism of the reactions discussed here is similar also in the double strand but that the results obtained on TpT cannot be directly translated to DNA. In DNA, indeed, the conformational equilibrium between the ring conformers is not the same as in the  $(dT)_{20}$  single strand, the steric hindrances due to the presence of interstrand hydrogen bonds is larger, and environmental effects (both static and dynamic) are different with respect to single strands, which are more exposed to solvent. It is also important to remember that the phosphoribose backbone is very flexible and therefore the stacking geometry in a double helix and in a single strand could be different.

Our results are also consistent with the decrease of the photodimerization yield in the presence of purine residues flanking the TT step in single and double strands.<sup>8</sup> As already suggested,<sup>8</sup> the formation of  $T \rightarrow$  purine CT exciplexes could decrease the population of the TT exciton involved in  $T<>T$  formation. Interestingly, the formation of CT excited states does not significantly depend on the presence of strongly stacked structures,<sup>8</sup> in line with the conclusions of the present study.

## 5. CONCLUSION

In this study we report a fully quantum mechanical study of the main photochemical and photophysical decay routes in aqueous solution of TpT deoxy-dinucleotide and of its locked analogues, characterizing five different representative backbone conformers: C3C3, C2C3, C3C2, C2C2 and C2C1.

Our computational approach, based on PCM/TD-M052X calculations, is able to reproduce the effect of the stacking on the spectral behavior of the dinucleotide. The computed absorption and ECD spectra of TpT (and of TpTNa) are indeed in good agreement with their experimental counterpart, suggesting that they can provide a solid base for identifying the position of the different electronic transitions in the broad experimental absorption spectrum.

Our study confirms that the backbone conformation modulates the ground state stacking geometry and, therefore the distance between the atoms involved in the main photochemical reaction. Though being fully consistent and supporting the hypothesis that  $T<>T$  formation occurs on a barrierless path on the lowest singlet excited state and its yield is governed by ground state conformation, our results clearly show that a more complex mechanism is operative. Indeed, different backbone conformations lead to different excited state properties. In particular, the reaction leading to 6-4TT formation, which is not barrierless and proceeds on the potential energy surface of the  $5'T^+ \rightarrow 3'T^-$  CT state, is more sensitive to static and dynamical environmental effects than to the initial ground state geometry. “Neutral exciton” and CT states could also interconvert (depending, for example, on backbone fluctuations changing the stacking distance), and this



process could also modulate the experimental photoproducts yield, especially for the slowest 6-4TT reaction.

Polynucleotides in solution are complex systems, posing huge difficulties to both experimental and computational studies, and additional work is therefore necessary to completely unveil and, hopefully, “manage” all the processes involved in DNA photodamage. On the other hand, the results recently obtained by using different, experimental and computational, methods are encouraging and the possible integration between quantum mechanical studies, molecular dynamics simulation, and purposely tailored studies (for example, checking the involvement of CT states in the 6-4TT formation or studying the reactivity of sequences containing only one locked residue) is promising.

## ■ ASSOCIATED CONTENT

### Supporting Information

Further information on quantum mechanical calculations. Detailed description of the excited state deactivation paths for different conformers. Tables of excitation energies and oscillator strengths, structural features, and absorption energies. Figures of molecular structures, absorption spectra, and the minimum energy path. Cartesian coordinates of the most relevant points of the PES. Complete Gaussian reference (ref 62 in the manuscript, ref 30 in the Supporting Information). This material is available free of charge via the Internet at <http://pubs.acs.org>.

## ■ AUTHOR INFORMATION

### Corresponding Author

\*E-mail: [robimp@unina.it](mailto:robimp@unina.it).

### Notes

The authors declare no competing financial interest.

## ■ ACKNOWLEDGMENTS

The author thanks Dr. D. Markovitsi and Dr. A. Banyasz for very useful discussion and for giving access to several unpublished results and MIUR (PRIN 2008 and FIRB Futuro in Ricerca) for financial support.

## ■ REFERENCES

- (1) Cadet, J.; Vigny, P. In *The Photochemistry of Nucleic Acids*; Morrison, H., Ed.; Wiley: New York, 1990.
- (2) Taylor, J. S. *Acc. Chem. Res.* **1994**, *27*, 76.
- (3) Schreier, W. J.; Schrader, T. E.; Kohler, F. O.; Gilch, P.; Crespo-Hernandez, C. E.; Swaminathan, V. N.; Carell, T.; Zinth, W.; Kohler, B. *Science* **2007**, *315*, 625.
- (4) Schreier, W. J.; Kubon, J.; Regner, N.; Haiser, K.; Schrader, T. E.; Zinth, W.; Clivio, P.; Gilch, P. *J. Am. Chem. Soc.* **2009**, *131*, 5038.
- (5) Marguet, S.; Markovitsi, D. *J. Am. Chem. Soc.* **2005**, *127*, 5780.
- (6) Hariharan, M.; Lewis, F. D. *J. Am. Chem. Soc.* **2008**, *130*, 11870.
- (7) Pan, Z.; Chen, J.; Schreier, W. J.; Kohler, B.; Lewis, F. D. *J. Phys. Chem. B* **2012**, *116*, 698–704.
- (8) Pan, Z.; Hariharan, M.; Arkin, J. D.; Jalilov, A. S.; McCullagh, M.; Schatz, G. C.; Lewis, F. D. *J. Am. Chem. Soc.* **2011**, *133*, 20793–20798.
- (9) Pan, Z.; McCullagh, M.; Schatz, G. C.; Lewis, F. D. *J. Phys. Chem. Lett.* **2011**, *2*, 1432.
- (10) Douki, T.; Court, M.; Sauvaigo, S.; Odin, F.; Cadet, J. *J. Biol. Chem.* **2000**, *275*, 11678.
- (11) Kwok, W. M.; Ma, C.; Phillips, D. L. *J. Am. Chem. Soc.* **2008**, *130*, 5131–5139.
- (12) (a) Cuquerella, M. C.; Lhiaubet-Vallet, V.; Cadet, J.; Miranda, M. A. *Acc. Chem. Res.* **2012**, *45*, 1558–1570. (b) Bosca, F.; Lhiaubet-Vallet, V.; Cuquerella, M. C.; Castell, J. V.; Miranda, M. A. *J. Am. Chem. Soc.* **2006**, *128*, 63186319.
- (13) Desnoux, C.; Babu, B. R.; McLriou, C.; Mayo, J. U. O.; Favre, A.; Wengel, J.; Clivio, P. *J. Am. Chem. Soc.* **2008**, *130*, 30–31.
- (14) Santini, G. P. H.; Pakleza, C.; Auffinger, P.; Moriou, C.; Favre, A.; Clivio, P.; Cognet, J. A. C. *J. Phys. Chem. B* **2007**, *111*, 9400–9409.
- (15) Ostrowski, T.; Maurizot, J.-C.; Adeline, M.-T.; Fourrey, J.-L.; Clivio, P. *J. Org. Chem.* **2003**, *68*, 6502–6510.
- (16) Lemaire, D.; Ruzsicska, B. P. *Photochem. Photobiol.* **1993**, *57*, 755.
- (17) Law, Y. K.; Azadi, J.; Crespo-Hernandez, C. E.; Olmon, E.; Kohler, B. *Biophys. J.* **2008**, *94*, 3590.
- (18) Johnson, A. T.; Wiest, O. *J. Phys. Chem. B* **2007**, *111*, 14398.
- (19) Hariharan, M.; McCullagh, M.; Schatz, G. C.; Lewis, F. D. *J. Am. Chem. Soc.* **2010**, *132*, 12856.
- (20) McCullagh, M.; Hariharan, M.; Lewis, F. D.; Markovitsi, D.; Douki, T.; Schatz, G. C. *J. Phys. Chem. B* **2010**, *114*, 5215–5221.
- (21) Onidas, D.; Markovitsi, D.; Marguet, S.; Sharonov, A.; Gustavsson, T. *J. Phys. Chem. B* **2002**, *106*, 11367–11374.
- (22) Banyasz, A.; Vaya, L.; Changelnet-Barret, P.; Gustavsson, T.; Douki, T.; Markovitsi, D. *J. Am. Chem. Soc.* **2011**, *133*, 5163–5165.
- (23) Boggio-Pasqua, M.; Groenhof, G.; Schaefer, L. V.; Grubmüller, H.; Robb, M. A. *J. Am. Chem. Soc.* **2007**, *129*, 10996.
- (24) Blancafort, L.; Migani, A. *J. Am. Chem. Soc.* **2007**, *129*, 14540–14541.
- (25) Serrano-Perez, J. J.; Gonzalez-Ramirez, I.; Coto, P. B.; Merchan, M.; Serrano-Andres, L. *J. Phys. Chem. B* **2008**, *112*, 14096.
- (26) Climent, T.; Gonzalez-Ramirez, I.; Gonzalez-Luque, R.; Merchan, M.; Serrano-Andres, L. *J. Phys. Chem. Lett.* **2010**, *1*, 2072–2076.
- (27) Du, Q.; Zhao, H.; Song, D.; Liu, K.; Su, H. *J. Phys. Chem. B* **2012**, *116*, 11117–11123.
- (28) Zhang, R. B.; Eriksson, L. A. *J. Phys. Chem. B* **2006**, *110*, 7556–7562.
- (29) Yang, Z. B.; Zhang, R. B.; Eriksson, L. A. *Phys. Chem. Chem. Phys.* **2011**, *13*, 8961–8966.
- (30) Varghese, A. J.; Wang, S. *Science* **1967**, *156*, 955.
- (31) Banyasz, A.; Douki, T.; Improta, R.; Gustavsson, T.; Onidas, D.; Vayá, I.; Perron, M.; Markovitsi, D. *J. Am. Chem. Soc.* **2012**, *134*, 14834–14845.
- (32) (a) Crespo-Hernandez, C. E.; Cohen, B.; Hare, P. M.; Kohler, B. *Chem. Rev.* **2004**, *104*, 1977–2020. (b) Middleton, C. T.; de La Harpe, K.; Su, C.; Law, Y. K.; Crespo-Hernandez, C. E.; Kohler, B. *Annu. Rev. Phys. Chem.* **2009**, *60*, 217.
- (33) Gustavsson, T.; Improta, R.; Markovitsi, D. *J. Phys. Chem. Lett.* **2010**, *1*, 2025.
- (34) Gustavsson, T.; Banyasz, A.; Lazzarotto, E.; Markovitsi, D.; Scalmani, G.; Frisch, M. J.; Barone, V.; Improta, R. *J. Am. Chem. Soc.* **2006**, *128*, 607.
- (35) Santoro, F.; Barone, V.; Gustavsson, T.; Improta, R. *J. Am. Chem. Soc.* **2006**, *128*, 16312–16322.
- (36) Hare, P. M.; Crespo-Hernandez, C. E.; Kohler, B. *Proc. Nat. Acad. Sci. U.S.A.* **2007**, *104*, 435.
- (37) (a) Kang, H.; Lee, K. T.; Jung, B.; Ko, Y. J.; Kim, S. K. *J. Am. Chem. Soc.* **2002**, *124*, 12958. (b) Canuel, C.; Mons, M.; Piuze, F.; Tardivel, B.; Dimicoli, I.; Elhanine, M. *J. Chem. Phys.* **2005**, *122*, 074316. (c) Ullrich, S.; Schultz, T.; Zgierski, M. Z.; Stolow, A. *Phys. Chem. Chem. Phys.* **2004**, *6*, 2796. (d) Gonzalez-Vazquez, J.; Gonzalez, L.; Samoylova, E.; Schultz, T. *Phys. Chem. Chem. Phys.* **2009**, *11*, 3927. (e) Busker, M.; Nispel, M.; Haber, T.; Kleinermanns, K.; Etinski, M.; Fleig, T. *ChemPhysChem* **2008**, *9*, 1570. (f) Gustavsson, T.; Sarkar, N.; Lazzarotto, E.; Markovitsi, D.; Improta, R. *Chem. Phys. Lett.* **2006**, *429*, 551.
- (38) (a) Improta, R.; Barone, V.; Lami, A.; Santoro, F. *J. Phys. Chem. B* **2009**, *113*, 14491. (b) Asturiol, D.; Lasorne, B.; Robb, M. A.; Blancafort, L. *J. Phys. Chem. A* **2009**, *113*, 10211. (c) Asturiol, D.; Lasorne, B.; Worth, G. A.; Robb, M. A.; Blancafort, L. *Phys. Chem. Chem. Phys.* **2010**, *12*, 4949. (d) Perun, S.; Sobolewski, A. L.; Domcke, W. *J. Phys. Chem. A* **2006**, *110*, 13238. (e) Merchan, M.; Gonzalez-

- Luque, R.; Climent, T.; Serrano-Andres, L.; Rodriguez, E.; Reguero, M.; Pelaez, D. *J. Phys. Chem. B* **2006**, *110*, 26471. (f) Szymczak, J. J.; Barbatti, M.; Soo Hoo, J. T.; Adkins, J. A.; Windus, T. L.; Nachtigallova, D.; Lischka, A. *J. Phys. Chem. A* **2009**, *113*, 12686. (g) Hudock, H. R.; Levine, B. G.; Thompson, A. L.; Satzger, H.; Townsend, D.; Gador, N.; Ullrich, S.; Stolow, A.; Martinez, T. J. *J. Phys. Chem. A* **2007**, *111*, 8500. (h) Lan, Z.; Fabiano, E.; Thiel, W. *J. Phys. Chem. B* **2009**, *113*, 3548. (i) Etinski, M.; Fleig, T.; Marian, C. M. *J. Phys. Chem. A* **2009**, *113*, 11809.
- (39) Picconi, D.; Barone, V.; Lami, A.; Santoro, F.; Improta, R. *ChemPhysChem* **2011**, *12*, 1957–1968.
- (40) Improta, R.; Barone, V. *Angew. Chem.* **2011**, *50*, 12016.
- (41) Santoro, F.; Barone, V.; Improta, R. *J. Am. Chem. Soc.* **2009**, *131*, 15232–15245.
- (42) Dargiewicz, M.; Biczysko, M.; Improta, R.; Barone, V. *Phys. Chem. Chem. Phys.* **2012**, *14*, 8981–8989.
- (43) Santoro, F.; Barone, V.; Improta, R. *ChemPhysChem* **2008**, *9*, 2531–2537.
- (44) Improta, R. *Phys. Chem. Chem. Phys.* **2008**, *10*, 2656–2664.
- (45) Zhao, Y.; Schultz, N. E.; Truhlar, D. G. *J. Chem. Theor. Comput.* **2006**, *2*, 364.
- (46) Zhao, Y.; Truhlar, D. G. *Acc. Chem. Res.* **2008**, *41*, 157–167.
- (47) Aquino, A.J.A.; Nachtigallova, D.; Hobza, P.; Truhlar, D. G.; Hattig, C.; Lischka, H. *J. Comput. Chem.* **2011**, *32*, 1217–1227.
- (48) Dreuw, A.; Head-Gordon, M. *Chem. Rev.* **2005**, *105*, 4009.
- (49) Lange, A. W.; Herbert, J. M. *J. Am. Chem. Soc.* **2009**, *131*, 3913–3922.
- (50) Perun, S.; Sobolewski, A. L.; Domcke, W. *J. Phys. Chem. A* **2006**, *110*, 9031.
- (51) Improta, R.; Barone, V. *Theor. Chem. Acc.* **2008**, *120*, 491–497.
- (52) (a) Adamo, C.; Barone, V. *J. Chem. Phys.* **1999**, *110*, 6158.
- (53) Zhao, Y.; Truhlar, D. G. *Theor. Chem. Acc.* **2008**, *120*, 215–241.
- (54) (a) Miertus, S.; Scrocco, E.; Tomasi, J. *J. Chem. Phys.* **1981**, *55*, 117. (b) Tomasi, J.; Mennucci, B.; Cammi, R. *Chem. Rev.* **2005**, *105*, 2999.
- (55) Improta, R. UV-Visible Absorption and Emission Energies in Condensed phase by PCM-TD-DFT methods. In *Computational Strategies for Spectroscopy: from Small Molecules to Nanosystems*; Barone, V., Ed.; John Wiley & Sons: Chichester, U.K., 2011; pp 39–76.
- (56) Scalmani, G.; Frisch, M. J.; Mennucci, B.; Tomasi, J.; Cammi, R.; Barone, V. *J. Chem. Phys.* **2006**, *124*, 094107.
- (57) Improta, R.; Barone, V.; Scalmani, G.; Frisch, M. J. *J. Chem. Phys.* **2006**, *125*, 54103.
- (58) Improta, R.; Scalmani, G.; Frisch, M. J.; Barone, V. *J. Chem. Phys.* **2007**, *127*, 74504.
- (59) Onidas, D.; Gustavsson, T.; Lazzarotto, E.; Markovitsi, D. *J. Phys. Chem. B* **2007**, *111*, 9644–9650.
- (60) Avila Ferrer, F. J.; Improta, R.; Santoro, F.; Barone, V. *Phys. Chem. Chem. Phys.* **2011**, *13*, 17007.
- (61) Marcus, R. A. *J. Chem. Phys.* **1965**, *43*, 1261.
- (62) Frisch, M. J.; et al. *Gaussian 09*; Gaussian, Inc.: Wallingford, CT, 2009.
- (63) (a) Tapavicza, E.; Tavernelli, I.; Rothlisberger, U. *Phys. Rev. Lett.* **2007**, *98*, 023001. (b) Tapavicza, E.; Tavernelli, I.; Rothlisberger, U.; Filippi, C.; Casida, M. E. *J. Chem. Phys.* **2008**, *129*, 124108.
- (64) Levine, B. G.; Ko, C.; Quenneville, J.; Martinez, T. J. *Mol. Phys.* **2006**, *104*, 1039.
- (65) Gonzales, L.; Escudero, D.; Serrano-Andres, L. *ChemPhysChem* **2012**, *13*, 28–51.
- (66) Haiser, K.; Fingerhut, B. P.; Heil, K.; Glas, A.; Herzog, T. T.; Pilles, B. M.; Schreier, W. J.; Zinth, W.; de Vivie-Riedle, R.; Carell, T. *Angew. Chem. Int. Ed.* **2012**, *51*, 408.
- (67) Churchill, C. D. M.; Wetmore, S. D. *Phys. Chem. Chem. Phys.* **2011**, *13*, 16373–16383.
- (68) (a) Improta, R.; Barone, V.; Santoro, F. *Angew. Chem., Int. Ed.* **2007**, *46*, 405–408. (b) Improta, R.; Barone, V.; Santoro, F. *J. Phys. Chem. B* **2007**, *111*, 14080. (c) Santoro, F.; Improta, R.; Lami, A.; Bloino, J.; Barone, V. *J. Chem. Phys.* **2007**, *126*, 084509. (d) Santoro, F.; Lami, A.; Improta, R.; Barone, V. *J. Chem. Phys.* **2007**, *126*, 184102.
- (69) Schreiber, M.; Silva, M. R. J.; Sauer, S. P. A.; Thiel, W. *J. Chem. Phys.* **2008**, *128*, 134110.
- (70) Szalay, P. G.; Watson, T.; Perera, A.; Lotrich, V. F.; Bartlett, R. J. *J. Phys. Chem. A* **2012**, *116*, 6702–6710.
- (71) (a) Biemann, L.; Kovalenko, S. A.; Kleinermanns, K.; Mahrwald, R.; Markert, M.; Improta, R. *J. Am. Chem. Soc.* **2011**, *133*, 19664–19667. (b) Dargiewicz, M.; Biczysko, M.; Roberto Improta, R.; Barone, V. *Phys. Chem. Chem. Phys.* **2012**, *14*, 8981–8989.
- (72) (a) Burghardt, I.; Hynes, J. T. *J. Phys. Chem. A* **2006**, *110*, 11411–11423. (b) Laage, D.; Burghardt, I.; Hynes, T. J. Non-equilibrium Solvation and Conical Intersections. In *Continuum Solvation Models in Chemical Physics: Theory and Application*; Cammi, R.; Mennucci, B., Eds.; Wiley-VCH: Weinheim, 2007; pp 429.
- (c) Toniolo, A.; Olsen, S.; Manohar, L.; Martnez, T. J. *Faraday Discuss.* **2004**, *127*, 149–63.
- (73) Improta, R.; Santoro, F.; Barone, V.; Lami, A. *J. Phys. Chem. A* **2009**, *113*, 15346–15354.
- (74) Yuan, S.; Zhang, W.; Liu, L.; Dou, Y.; Fang, W.; Lo, G. V. *J. Phys. Chem. A* **2011**, *115*, 13291–13297.